# Supplementary Notes: Probing Rotational Decoherence with a Trapped-Ion Planar Rotor

Neil Glikin,[1,2] Benjamin A. Stickler,[3] Ryan Tollefsen,[1,2] Sara Mouradian,[4]
Neha Yadav,[1,2] Erik Urban,[1,*] Klaus Hornberger,[5] and Hartmut Häffner[1,2]

[1] *Department of Physics, University of California, Berkeley, Berkeley, California 94720, USA*
[2] *Challenge Institute for Quantum Computation, University of California, Berkeley, Berkeley, California 94720, USA*
[3] *Institute for Complex Quantum Systems, Ulm University, Albert-Einstein-Allee 11, 89069 Ulm, Germany*
[4] *Department of Electrical and Computer Engineering, University of Washington, Seattle, Washington 98195, USA*
[5] *University of Duisburg-Essen, Faculty of Physics, Lotharstraße 1, 47057 Duisburg, Germany*

## I. THEORETICAL DESCRIPTION

### A. Derivation of the master equation

We consider a planar rigid rotor formed by two ions with charges $e$ at positions $r_{1,2} = z\mathbf{e}_z \pm r\mathbf{e}_\rho(\phi)$, where $z$ is the height above the surface trap, $2r$ is the ion separation, and the angle $\phi$ describes the rotor orientation. The potential energy of the rotor in the quadrupole potential follows as

$$V(\phi) = -er^2\mathbf{e}_\rho(\phi)\cdot[\nabla\otimes\mathbf{E}(z\mathbf{e}_z,t)]\,\mathbf{e}_\rho(\phi), \tag{S1}$$

where $\mathbf{E}(\mathbf{r},t)$ is the local field strength at time $t$. The vector gradient $\nabla\otimes\mathbf{E}(z\mathbf{e}_z,t)$ is symmetric and traceless, and determined by the trap geometry. Using that $L_\pm = e^{\pm i\phi}$, this potential energy can be rewritten up to an additive constant as

$$V_t(\phi) = \frac{er^2}{4}\left(\varepsilon_t L_+^2 + \varepsilon_t^* L_-^2\right), \tag{S2}$$

where we defined the complex-valued combination of field gradients

$$\varepsilon_t = -\partial_x E_x + \partial_y E_y + 2i\partial_x E_y, \tag{S3}$$

whose magnitude is determined by the trapping geometry as well as the time-dependent voltage applied to the control electrodes.

The quantum state $|\psi_t\rangle$ of the rotor evolves according to the Schrödinger equation with the free Hamiltonian $H_0 = L_z^2/2I$ and the potential (S2). Transformation to the interaction picture $|\psi_t\rangle = \exp(-iH_0t/\hbar)\,|\chi_t\rangle$ shows that the rotor evolves according to the interaction picture potential $\widetilde{V}_t = \exp(iH_0t/\hbar)V_t\exp(-iH_0t/\hbar)$, which can be further evaluated by using that

$$L_\pm^2(t) = e^{iH_0t/\hbar}L_\pm^2 e^{-iH_0t/\hbar} = e^{2i\hbar t/I}L_\pm^2 e^{\pm 2itL_z/I}, \tag{S4}$$

as follows from the commutation relations $[L_z, L_\pm] = \pm\hbar L_\pm$ and $L_\pm L_\mp = \mathbb{I}$. The interaction picture Schrödinger equation is thus given by $i\hbar\partial_t\,|\chi_t\rangle = \widetilde{V}_t\,|\chi_t\rangle$ with

$$\widetilde{V}_t = \frac{er^2}{4}\left(e^{2i\hbar t/I}\varepsilon_t L_+^2 e^{2itL_z/I} + \text{h.c.}\right). \tag{S5}$$

We now integrate this Schrödinger equation over the time interval $\Delta t \gg 1/\omega_{\rm rot}$ and iterate the resulting integral equation twice to obtain

$$\begin{aligned}|\chi_{t+\Delta t}\rangle = |\chi_t\rangle &- \frac{i}{\hbar}\int_t^{t+\Delta t} dt'\widetilde{V}_{t'}\,|\chi_t\rangle \\ &- \frac{1}{\hbar^2}\int_t^{t+\Delta t} dt'\int_t^{t'} dt''\widetilde{V}_{t'}\widetilde{V}_{t''}\,|\chi_{t''}\rangle\,.\end{aligned} \tag{S6}$$

To express that $|\chi_t\rangle$ evolves little in $\Delta t$, we approximate $|\chi_{t''}\rangle \simeq |\chi_t\rangle$.

This equation describes how the dynamics of the pure state $|\chi_t\rangle$ is influenced by the time-dependent voltage applied to the control electrodes. This voltage is chosen randomly, so that the rotor state is described by the density operator $\widetilde{\rho} = \mathbb{E}[|\chi_t\rangle\langle\chi_t|]$, where $\mathbb{E}$ denotes the ensemble average over many repetitions of the experiment. The equation of motion for $\widetilde{\rho}$ can be derived by calculating

$$\Delta\widetilde{\rho} = \mathbb{E}(|\chi_{t+\Delta t}\rangle\langle\chi_{t+\Delta t}|) - |\chi_t\rangle\langle\chi_t| \tag{S7}$$

by inserting Eq. (S6), which yields

$$\begin{aligned}\Delta\widetilde{\rho} =& \frac{1}{\hbar^2}\int_t^{t+\Delta t} dt'\int_t^{t+\Delta t} dt''\mathbb{E}\left(\widetilde{V}_{t'}\widetilde{\rho}\widetilde{V}_{t''}\right) \\ &- \frac{1}{\hbar^2}\int_t^{t+\Delta t} dt'\int_t^{t'} dt''\left\{\mathbb{E}\left(\widetilde{V}_{t'}\widetilde{V}_{t''}\right),\widetilde{\rho}\right\}.\end{aligned} \tag{S8}$$

Here, $\{A,B\} = AB + BA$ denotes the anticommutator.

The time integrals appearing in Eq. (S8) can be calculated for rapidly revolving rotor states $|\chi_t\rangle$, which are localized in angular momentum close to the quantum number $\overline{\ell} = I\omega_{\rm rot}/\hbar \gg 1$ with angular momentum spread $\sigma_\ell \ll \ell$. Since this implies $\exp(\pm 2itL_z/I)\,|\chi_t\rangle \simeq e^{\pm 2i\omega_{\rm rot}t}\,|\chi_t\rangle$ one is left with the integrals

$$\int_t^{t+\Delta t} dt'\int_t^{t+\Delta t} dt''\mathbb{E}(\varepsilon_{t'}\varepsilon_{t''}^*)e^{2i\omega_{\rm rot}(t'-t'')} \simeq \Delta t S_\varepsilon(2\omega_{\rm rot}) \tag{S9a}$$

---

* Current address: Exponent, Inc., Electrical Engineering and Computer Science Practice, Warrenville, IL

and

$$\int_t^{t+\Delta t} dt' \int_t^{t'} dt'' \mathbb{E}(\varepsilon_{t'}\varepsilon^*_{t''}) e^{2i\omega_{\rm rot}(t'-t'')} \simeq \frac{\Delta t}{2} S_\varepsilon(2\omega_{\rm rot}) \tag{S9b}$$

upon inserting (S5) and neglecting rapidly rotating terms $\exp[\pm i 2\omega_{\rm rot}(t'+t'')] \simeq 0$ in the rotating-wave approximation. In both integrals we used that $\varepsilon_t$ is described by a real, stationary, and time-inversion-invariant stochastic process with zero mean, multiplied by a fixed complex phase factor (as determined by (S3)), to identify the power spectral density

$$S_\varepsilon(\omega) = \int_{-\infty}^{\infty} d\tau \mathbb{E}(\varepsilon_t \varepsilon^*_{t-\tau}) e^{i\omega\tau}. \tag{S10}$$

The statistical properties of the the applied voltage directly translate to those of $\varepsilon_t$ since retardation effects in the field propagation can be neglected at the short distances of the experiment. The time interval $\Delta t$ will be taken large compared to the decay time of the noise correlations. Moreover, the noise filter bandwidth of 20 kHz is large in comparison to the width of the rotation frequencies $\hbar\sigma_\ell/I \simeq 1\,$kHz, justifying the approximation before Eq. (S9).

Inserting the integrals (S9) into equation (S8) shows that the ensemble-averaged quantum state follows the Markovian master equation

$$\partial_t \widetilde{\rho} \simeq \frac{\Delta\widetilde{\rho}}{\Delta t} = \frac{D}{4\hbar^2}\left(L_+^2\widetilde{\rho}L_-^2 + L_-^2\widetilde{\rho}L_+^2 - 2\widetilde{\rho}\right), \tag{S11}$$

with the diffusion coefficient $D$ given by $e^2r^4S_\varepsilon(2\omega_{\rm rot})/4$ as stated in the main text. Transforming back to the Schrödinger picture yields (under the same assumptions as above) the master equation (2).

Note that the diffusion coefficient can also be obtained in a classical picture. Starting from the equation of motion in the noisy potential (S2),

$$\dot{L}_z = -i\frac{er^2}{2}\left(\varepsilon_t e^{2i\phi} - \varepsilon_t^* e^{-2i\phi}\right), \tag{S12}$$

together with $\dot\phi = L_z/I$, it follows that $\mathbb{E}(L_z) = \text{const}$. In order to obtain the diffusion coefficient, we first formally solve (S12) for a time step $\Delta t$ in the co-rotating frame $\phi \to \phi + \omega_{\rm rot}t$,

$$\begin{aligned} L_z(t+\Delta t) =& L_z(t) - i\frac{er^2}{2}\int_t^{t+\Delta t} dt' \Big(\varepsilon_{t'} e^{2i\phi + 2i\omega_{\rm rot}t'} \\ & - \varepsilon^*_{t'} e^{-2i\phi - 2i\omega_{\rm rot}t'}\Big). \end{aligned} \tag{S13}$$

Here we use that $\phi(t') \simeq \phi(t)$ under the same approximation as after (S8). A rotating wave approximation and (S9a) yield the second moment

$$\begin{aligned} &\mathbb{E}[L_z^2(t+\Delta t)] - \mathbb{E}[L_z^2(t)] \\ &\quad\simeq \frac{e^2r^4}{2}\int_t^{t+\Delta t} dt' \int_t^{t+\Delta t} dt'' \mathbb{E}(\varepsilon_{t'}\varepsilon^*_{t''}) e^{2i\omega_{\rm rot}(t'-t'')} \\ &\quad\simeq 2D\Delta t. \end{aligned} \tag{S14}$$

Drawing the limit $\Delta t \to 0$, we thus obtain $\partial_t \mathbb{E}(L_z^2) = 2D$ as also implied by the quantum master equation (2). While angular momentum diffusion can be understood classically, the observed decoherence of rotational superpositions is a genuine signature of the quantum master equation (2).

### B. Time evolution in the noise field

The time evolution under the master equation (2) can be determined by using Eq. (S6) for a pure state $|\chi_t\rangle$ and then calculating the ensemble average over many repetitions of the experiment. Specifically, approximating $|\chi_{t''}\rangle$ on the right hand side by $|\chi_t\rangle$ (see above), the operator

$$\begin{aligned} W(t) =& \mathbb{I} - \frac{i}{\hbar}\int_t^{t+\Delta t} dt' \widetilde{V}_{t'} \\ & - \frac{1}{\hbar^2}\int_t^{t+\Delta t} dt' \int_t^{t'} dt'' \widetilde{V}_{t'}\widetilde{V}_{t''} \end{aligned} \tag{S15}$$

propagates the state over the time interval $\Delta t$, $|\chi_{t+\Delta t}\rangle = W(t)\,|\chi_t\rangle$. Concatenating $N = t/\Delta t \gg 1$ of these timesteps, we can express the Schrödinger-picture state at time $t$ as

$$|\psi_t\rangle = e^{-iH_0t/\hbar} U_t\,|\psi_0\rangle\,, \tag{S16}$$

where $|\psi_0\rangle$ is the initial state and

$$U_t \simeq W(t-\Delta t)\cdots W(\Delta t)\,W(0)\,, \tag{S17}$$

When calculating expectation values in the ensemble average, we can use that the random fields $\varepsilon_t$ are uncorrelated between different time intervals $[n\Delta t, (n+1)\Delta t]$. One can thus decompose the ensemble average over the random noise trajectory $\mathbb{E}(\cdot)$ by the product of ensemble averages $\mathbb{E}_n(\cdot)$ at fixed times $t_n = n\Delta t$, so that

$$\mathbb{E}(\cdot) = \lim_{N\to\infty} \mathbb{E}_{N-1}(\mathbb{E}_{N-2}(\cdots \mathbb{E}_0(\cdot))). \tag{S18}$$

This property will be used below to determine the outcome of the Ramsey interference protocol.

The Ramsey scheme discussed below requires the time evolution (S16) of a coherent rotor state $|\Psi_\ell\rangle$ characterized by a mean angular momentum quantum number $\ell$ and width $\sigma_\ell$ with $\ell \gg \sigma_\ell \gg 1$. Using that $L_\pm^2(t)\,|\Psi_\ell\rangle \simeq e^{\pm 4i\ell\omega_{\rm r}t}\,|\Psi_\ell\rangle$, with $\omega_{\rm r} = \hbar/2I$, yields

$$\begin{aligned} |\psi_t\rangle &\simeq u_\ell(t) e^{-iH_0t/\hbar}\,|\Psi_\ell\rangle \\ &\simeq u_\ell(t) e^{i\ell^2\omega_{\rm r}t} e^{-i2\ell\omega_{\rm r}tL_z/\hbar}\,|\Psi_\ell\rangle\,. \end{aligned} \tag{S19}$$

Here, $u_\ell(t)$ is the c-number obtained by replacing in $U_t$ all operators $L_\pm^2(t_n)$ by $\exp(\pm 4i\ell\omega_{\rm r}t_n)$. In the second expression, the unitary operator $\exp(-i2\ell\omega_{\rm r}tL_z/\hbar)$ serves to displace the rotor state by the angle $2\ell\omega_{\rm r}t$, while the global phase factor results from neglecting dispersion.

The Ramsey scheme also requires a generalization of (S19) for the the case of a coherent rotor state displaced by the angle $\varphi$. Using that

$$L_\pm^2(t)e^{-i\varphi L_z/\hbar} = e^{\pm 2i\varphi}e^{-i\varphi L_z/\hbar}L_\pm^2(t), \tag{S20}$$

we obtain

$$\begin{aligned}|\psi_t\rangle &\simeq u_\ell(t|\varphi)e^{-iH_0t/\hbar}e^{-i\varphi L_z/\hbar}|\Psi_\ell\rangle \\ &\simeq u_\ell(t|\varphi)e^{i\ell^2\omega_\mathrm{r}t}e^{-i(\varphi+2\ell\omega_\mathrm{r}t)L_z/\hbar}|\Psi_\ell\rangle\,. \end{aligned}\tag{S21}$$

Like above, the c-numbers $u_\ell(t|\varphi)$ are obtained by replacing in $U_t$ all operators $L_\pm^2(t_n)$ by $\exp[\pm 2i(\varphi+2\ell\omega_\mathrm{r}t_n)]$.

### C. Rabi pulses

This section derives the action of a Rabi pulse on the four internal levels and the rotational degrees of freedom of the two-ion rotor. We start with the light-matter Hamiltonian

$$H_\mathrm{L} = \sum_{j=1}^{2}\sigma_j^+ f_\mathrm{L}(\mathbf{r}_j,t) + \mathrm{h.c.}, \tag{S22}$$

where $\sigma_j^+ = |D\rangle_j\langle S|_j$ describes the excitation of the quadrupole transition of atom $j$, and $f_\mathrm{L}(\mathbf{r}_j,t)$ is determined by the relevant field gradient at the position of the $j$-th atom. Assuming plane-wave illumination with inclination $\theta$ to the rotor plane, we have

$$f_\mathrm{L}(\mathbf{r}_j,t) = \hbar g_0 e^{-i(kz\cos\theta+\omega t)}e^{i(-1)^j kr\sin\theta\cos\phi}, \tag{S23}$$

where $g_0$ is the coupling rate, $\omega$ is the laser frequency, and $k=\omega/c$. Using that

$$\langle\ell+\Delta\ell|\,e^{\pm ikr\sin\theta\cos\phi}\,|\ell\rangle = (\pm i)^{\Delta\ell}J_{\Delta\ell}(kr\sin\theta), \tag{S24}$$

one obtains

$$\begin{aligned}H_\mathrm{L} =&\hbar g_0 e^{-i(kz\cos\theta+\omega t)}\sum_{j=1}^{2}\sum_{\Delta\ell\in\mathbb{Z}}(-1)^{j\Delta\ell}i^{\Delta\ell} \\ &\times J_{\Delta\ell}(kr\sin\theta)\sigma_j^+L_+^{\Delta\ell} + \mathrm{h.c.},\end{aligned}\tag{S25}$$

The light-matter Hamiltonian (S25) can be further simplified by first transforming into the frame co-rotating with the laser field and then into the interaction picture with respect to $H_\mathrm{rot} = \hbar\Delta\omega(\sigma_1^+\sigma_1^- + \sigma_2^+\sigma_2^-) + H_0$, where $\Delta\omega = \omega_0-\omega$ denotes the laser detuning from the electronic transition frequency $\omega_0$. This yields

$$\begin{aligned}H_\mathrm{L}(t) =&e^{iH_\mathrm{rot}t/\hbar}H_\mathrm{L}e^{-iH_\mathrm{rot}t/\hbar} \\ =&\hbar g_0 e^{-ikz\cos\theta}\sum_{j=1}^{2}\sum_{\ell\in\mathbb{Z}}\sum_{\Delta\ell\in\mathbb{Z}}(-1)^{j\Delta\ell}i^{\Delta\ell}J_{\Delta\ell}(kr\sin\theta) \\ &\times e^{it[\Delta\omega+\Delta\ell(2\ell+\Delta\ell)\omega_\mathrm{r}]}\sigma_j^+\,|\ell+\Delta\ell\rangle\langle\ell| + \mathrm{h.c.}\end{aligned}\tag{S26}$$

For rapidly rotating states, where $2\ell+\Delta\ell\simeq 2\ell$, the laser frequency is tuned in resonance with the angular momentum transition $\Delta\ell$ by choosing $\omega\simeq\omega_0+2\ell\omega_\mathrm{r}\Delta\ell$, so that

$$H_\mathrm{L}(t) \simeq \hbar g\left[\sigma_1^+L_+^{\Delta\ell} + (-1)^{\Delta\ell}\sigma_2^+L_+^{\Delta\ell}\right] + \mathrm{h.c.}, \tag{S27}$$

where we defined

$$g = g_0 e^{-ikz\cos\theta}(-i)^{\Delta\ell}J_{\Delta\ell}(kr\sin\theta). \tag{S28}$$

The excitation of the atom's electronic state is thus accompanied by an angular momentum kick of strength $\Delta\ell$. Applying the laser field for a short time period $t$, as described by the unitary

$$\begin{aligned}U_\mathrm{L}(t) =&\exp\left[-igt\left(\sigma_1^+L_+^{\Delta\ell} + \mathrm{h.c.}\right)\right] \\ &\times\exp\left[-igt(-1)^{\Delta\ell}\left(\sigma_2^+L_+^{\Delta\ell} + \mathrm{h.c.}\right)\right],\end{aligned}\tag{S29}$$

gives rise to Rabi oscillations, which can be used to implement $\pi/2$-pulses and $\pi$-pulses. Specifically, choosing $gt=-i\pi/4$ implements a $\pi/2$-pulse,

$$\begin{aligned}X_{\pi/2} =&\frac{\mathbb{I}}{2} - \frac{\sigma_1^+ + (-1)^{\Delta\ell}\sigma_2^+}{2}L_+^{\Delta\ell} + \frac{\sigma_1^- + (-1)^{\Delta\ell}\sigma_2^-}{2}L_-^{\Delta\ell} \\ &+\frac{(-1)^{\Delta\ell}}{2}\left(\sigma_1^+\sigma_2^+L_+^{2\Delta\ell} + \sigma_1^-\sigma_2^-L_-^{2\Delta\ell}\right. \\ &\left.-\sigma_1^+\sigma_2^- - \sigma_1^-\sigma_2^+\right).\end{aligned}\tag{S30}$$

Likewise, choosing $gt=-i\pi/2$ gives the $\pi$-pulse

$$\begin{aligned}X_\pi =&(-1)^{\Delta\ell}\left(\sigma_1^+\sigma_2^+L_+^{2\Delta\ell} + \sigma_1^-\sigma_2^-L_-^{2\Delta\ell}\right. \\ &\left.-\sigma_1^+\sigma_2^- - \sigma_1^-\sigma_2^+\right).\end{aligned}\tag{S31}$$

### D. Ramsey scheme

The interferometer sequence, as sketched in Fig. 1, consists of the following steps:

(0) **Initialization**—The rotor is prepared in the coherent rotor state $|\Phi_0\rangle = \left|SS,\Psi_{\bar\ell}\right\rangle$ with mean angular momentum $\bar\ell\gg\sigma_\ell$.

(1) **Creation of the superposition**—At $t=0$, a $\pi/2$-pulse creates a superposition of angular momentum states $|\Phi_1\rangle = X_{\pi/2}|\Phi_0\rangle$. Direct application of Eq. (S30) yields the threefold superposition

$$|\Phi_1\rangle = \frac{1}{2}\left(|1\rangle - \sqrt{2}\,|2\rangle + |3\rangle\right), \tag{S32}$$

with the three orthonormal states

$$|1\rangle = \left|SS,\Psi_{\bar\ell}\right\rangle \tag{S33a}$$

$$|2\rangle = \frac{1}{\sqrt{2}}\left(|DS\rangle + (-1)^{\Delta\ell}|SD\rangle\right)\left|\Psi_{\bar\ell+\Delta\ell}\right\rangle \tag{S33b}$$

$$|3\rangle = (-1)^{\Delta\ell}\left|DD,\Psi_{\bar\ell+2\Delta\ell}\right\rangle \tag{S33c}$$

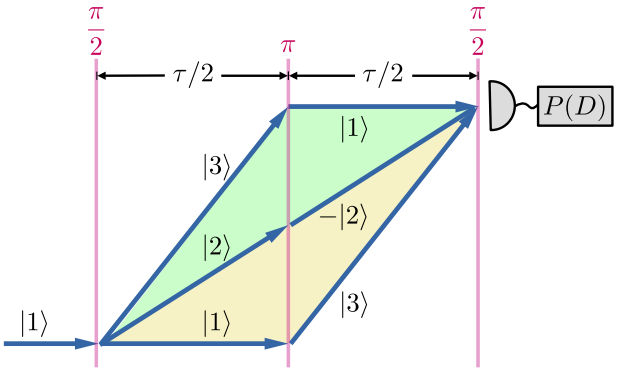


FIG. 1. Sketch of the rotational interferometer sequence consisting of the two $\pi/2$-pulses and an intermediate $\pi$-pulse to implement a Hahn echo at separation $\tau/2$. The three involved two-ion rotor states, defined in Eqs. (S33), revolve with mean angular momentum $\bar{\ell}$, $\bar{\ell}+\Delta\ell$, and $\bar{\ell}+2\Delta\ell$, respectively. The shaded regions indicate the coherences between superposition branches as read-out by the measurement of the mean excitation probability $P(D)$, see Eq. (S42).

The laser pulse thus entangles the two ion's internal state with that of the rotational degree of freedom. Whether $\Delta\ell$ is even or odd determines whether the $\pi/2$ pulse creates the even or odd superposition of $|DS\rangle$ and $|SD\rangle$.

(2) **Time evolution**—This is followed by a time evolution according to Eq. (S16) in presence of the environment until $t=\tau/2$, $|\Phi_2\rangle = e^{-iH_{\rm rot}\tau/2\hbar}U_{\tau/2}|\Phi_1\rangle$. Using the result (S19) yields

$$\begin{aligned}|\Phi_2\rangle =&\frac{1}{2}\left[a_{\bar{\ell}}T_{\bar{\ell}}|1\rangle - \sqrt{2}e^{-i\Delta\omega\tau/2}a_{\bar{\ell}+\Delta\ell}T_{\bar{\ell}+\Delta\ell}|2\rangle\right.\\ &\left.+e^{-i\Delta\omega\tau}a_{\bar{\ell}+2\Delta\ell}T_{\bar{\ell}+2\Delta\ell}|3\rangle\right].\end{aligned}\tag{S34}$$

Here, we introduced the weights

$$a_\ell = e^{i\ell^2\omega_{\rm r}\tau/2}u_\ell\left(\frac{\tau}{2}\right)\tag{S35}$$

and the angular displacement operators

$$T_\ell = \exp\left(-i\frac{\ell\omega_{\rm r}\tau L_z}{\hbar}\right)\tag{S36}$$

(3) **Hahn echo pulse**—At $t=\tau/2$, a $\pi$-pulse implements a Hahn echo $|\Phi_3\rangle = X_\pi|\Phi_2\rangle$. Using Eq. (S31) this becomes

$$\begin{aligned}|\Phi_3\rangle =&\frac{1}{2}\left[a_{\bar{\ell}}T_{\bar{\ell}}|3\rangle + e^{-i\Delta\omega\tau/2}\sqrt{2}a_{\bar{\ell}+\Delta\ell}T_{\bar{\ell}+\Delta\ell}|2\rangle\right.\\ &\left.+e^{-i\Delta\omega\tau}a_{\bar{\ell}+2\Delta\ell}T_{\bar{\ell}+2\Delta\ell}|1\rangle\right].\end{aligned}\tag{S37}$$

(4) **Time evolution**—This is followed by the second time evolution in presence of the environment until $t=\tau$, $|\Phi_4\rangle = e^{-iH_{\rm rot}\tau/2\hbar}U_{\tau/2}|\Phi_3\rangle$. Using Eq. (S21) yields

$$\begin{aligned}|\Phi_4\rangle =&\frac{1}{2}e^{-i\Delta\omega\tau}T^2_{\bar{\ell}+\Delta\ell}\left[b^{\bar{\ell}}_{\bar{\ell}+2\Delta\ell}a_{\bar{\ell}}|3\rangle + \sqrt{2}b^{\bar{\ell}+\Delta\ell}_{\bar{\ell}+\Delta\ell}a_{\bar{\ell}+\Delta\ell}|2\rangle\right.\\ &\left.+b^{\bar{\ell}+2\Delta\ell}_{\bar{\ell}}a_{\bar{\ell}+2\Delta\ell}|1\rangle\right],\end{aligned}\tag{S38}$$

where we abbreviated the weights

$$b^{\ell'}_\ell = e^{i\ell^2\omega_{\rm r}\tau/2}u_\ell\left(\frac{\tau}{2}\middle|\omega_{\rm r}\tau\ell'\right).\tag{S39}$$

Note that all states in the superposition (S38) are translated by the same angle $2(\bar{\ell}+\Delta\ell)\omega_{\rm r}\tau$, meaning that the interferometer can now be closed.

(5) **Closing of the interferometer**—A second $\pi/2$-pulse $|\Phi_5\rangle = X_{\pi/2}|\Phi_4\rangle$ yields

$$\begin{aligned}|\Phi_5\rangle =&\frac{1}{4}e^{-i\Delta\omega\tau}T^2_{\bar{\ell}+\Delta\ell}\left[\sqrt{2}\left(b^{\bar{\ell}}_{\bar{\ell}+2\Delta\ell}a_{\bar{\ell}} - b^{\bar{\ell}+2\Delta\ell}_{\bar{\ell}}a_{\bar{\ell}+2\Delta\ell}\right)|2\rangle\right.\\ &+\left(b^{\bar{\ell}}_{\bar{\ell}+2\Delta\ell}a_{\bar{\ell}} + 2b^{\bar{\ell}+\Delta\ell}_{\bar{\ell}+\Delta\ell}a_{\bar{\ell}+\Delta\ell} + b^{\bar{\ell}+2\Delta\ell}_{\bar{\ell}}a_{\bar{\ell}+2\Delta\ell}\right)|1\rangle\\ &\left.+\left(b^{\bar{\ell}}_{\bar{\ell}+2\Delta\ell}a_{\bar{\ell}} - 2b^{\bar{\ell}+\Delta\ell}_{\bar{\ell}+\Delta\ell}a_{\bar{\ell}+\Delta\ell} + b^{\bar{\ell}+2\Delta\ell}_{\bar{\ell}}a_{\bar{\ell}+2\Delta\ell}\right)|3\rangle\right]\end{aligned}\tag{S40}$$

(6) **Measurement**—Measuring the mean flourescence light of the two atoms yields the mean probability of being in the excited state,

$$\begin{aligned}P(D) =&\text{Prob}(DD) + \frac{1}{2}\left[\text{Prob}(DS) + \text{Prob}(SD)\right]\\ =&\frac{1}{2} + \frac{1}{2}\left[\text{Prob}(DD) - \text{Prob}(SS)\right].\end{aligned}\tag{S41}$$

Using the final state (S40) and averaging over many repetitions of the experiment yields

$$\begin{aligned}P(D) =&\frac{1}{2} - \frac{1}{4}\text{Re}\left[\mathbb{E}\left(b^{\bar{\ell}+\Delta\ell}_{\bar{\ell}+\Delta\ell}(b^{\bar{\ell}}_{\bar{\ell}+2\Delta\ell})^*\right)\mathbb{E}(a_{\bar{\ell}+\Delta\ell}a^*_{\bar{\ell}})\right.\\ &\left.+\mathbb{E}\left(b^{\bar{\ell}+\Delta\ell}_{\bar{\ell}+\Delta\ell}(b^{\bar{\ell}+2\Delta\ell}_{\bar{\ell}})^*\right)\mathbb{E}(a_{\bar{\ell}+\Delta\ell}a^*_{\bar{\ell}+2\Delta\ell})\right].\end{aligned}\tag{S42}$$

Here, we used that the coefficients $a_\ell$ and $b^{\ell'}_\ell$ are statistically uncorrelated as discussed in the context of Eq. (S18). Next, we will explicitly calculate the ensemble averages in Eq. (S42).

### E. Ensemble averaged signal

We are now in the position to evaluate the ensemble-averaged signal (S42) by using the decomposition (S17) and the rule (S18). We start with

$$\begin{aligned}\mathbb{E}(a_{\bar{\ell}+\Delta\ell}a^*_{\bar{\ell}}) =&\exp\left[i\frac{\omega_{\rm r}\tau}{2}\Delta\ell(2\bar{\ell}+\Delta\ell)\right]\\ &\times\mathbb{E}\left[u_{\bar{\ell}+\Delta\ell}\left(\frac{\tau}{2}\right)u^*_{\bar{\ell}}\left(\frac{\tau}{2}\right)\right].\end{aligned}\tag{S43}$$

The expectation value in the second line can be calculated by writing

$$\mathbb{E}\left[u_{\bar{\ell}+\Delta\ell}\left(\frac{\tau}{2}\right)u^*_{\bar{\ell}}\left(\frac{\tau}{2}\right)\right]=\prod_{n,n'=0}^{N}\mathbb{E}\left[w_{\bar{\ell}+\Delta\ell}(n\Delta t)w^*_{\bar{\ell}}(n'\Delta t)\right], \tag{S44}$$

where $\Delta t=\tau/2N$ with $N\gg 1$, and we defined

$$\begin{aligned}w_\ell(n\Delta t)=&1-\frac{i}{\hbar}\int_{n\Delta t}^{(n+1)\Delta t}dt' v_\ell(t')\\&-\frac{1}{\hbar^2}\int_{n\Delta t}^{(n+1)\Delta t}dt'\int_{n\Delta t}^{t'}dt'' v_\ell(t')v_\ell(t''),\end{aligned} \tag{S45}$$

with

$$v_\ell(t)=\frac{er^2}{4}(\varepsilon_t e^{4i\ell\omega_r t}+\text{c.c.}). \tag{S46}$$

This latter function is obtained by replacing $L^2_\pm(t)$ in the potential energy (S5) by the c-numbers $\exp(\pm 4i\ell\omega_r t)$.

Inserting Eq. (S45) into Eq. (S44) and using the same steps as in the derivation of the master equation yields

$$\begin{aligned}&\mathbb{E}\left[u_{\bar{\ell}+\Delta\ell}\left(\frac{\tau}{2}\right)u^*_{\bar{\ell}}\left(\frac{\tau}{2}\right)\right]\\&\simeq\prod_{n=0}^{N}\left[1-\frac{D\Delta t}{\hbar^2}\sin^2\left[\Delta\ell\,(2n+1)\,\omega_r\Delta t\right]\right]\\&\simeq\prod_{n=0}^{N}\exp\left[-\frac{D\Delta t}{\hbar^2}\sin^2\left[\Delta\ell\,(2n+1)\,\omega_r\Delta t\right]\right].\end{aligned} \tag{S47}$$

For $N\gg 1$ the sum in the exponent can be approximated by an integral, leading to

$$\begin{aligned}\mathbb{E}(a_{\bar{\ell}+\Delta\ell}a^*_{\bar{\ell}})\simeq&\exp\left(-\frac{D\tau}{4\hbar^2}\left[1-\text{sinc}\left(2\Delta\ell\omega_r\tau\right)\right]\right)\\&\times\exp\left[i\frac{\omega_r\tau}{2}\Delta\ell(2\bar{\ell}+\Delta\ell)\right].\end{aligned} \tag{S48}$$

In a similar fashion, one can evaluate the expectation value

$$\begin{aligned}\mathbb{E}(a_{\bar{\ell}+\Delta\ell}a^*_{\bar{\ell}+2\Delta\ell})\simeq&\exp\left(-\frac{D\tau}{4\hbar^2}\left[1-\text{sinc}\left(2\Delta\ell\omega_r\tau\right)\right]\right)\\&\times\exp\left[-i\frac{\omega_r\tau}{2}\Delta\ell(2\bar{\ell}+3\Delta\ell)\right]\end{aligned} \tag{S49}$$

It contains the same decoherence-induced decay as the expression above since only the relative angular momentum between the two superposition branches matters.

The expectation values containing $b^{\ell'}_\ell$ coefficients can be calculated by a straight-forward generalization replacing $v_\ell(t)$ by

$$v^{\ell'}_\ell(t)=\frac{er^2}{4}(\varepsilon_t e^{i2\ell'\omega_r\tau}e^{4i\ell\omega_r t}+\text{c.c.}). \tag{S50}$$

This yields

$$\begin{aligned}\mathbb{E}\left[b^{\bar{\ell}+\Delta\ell}_{\bar{\ell}+\Delta\ell}(b^{\bar{\ell}}_{\bar{\ell}+2\Delta\ell})^*\right]\simeq&\exp\left(-\frac{D\tau}{4\hbar^2}\left[1-\text{sinc}\left(2\Delta\ell\omega_r\tau\right)\right]\right)\\&\times\exp\left[-i\frac{\omega_r\tau}{2}\Delta\ell(2\bar{\ell}+3\Delta\ell)\right]\end{aligned} \tag{S51}$$

and

$$\begin{aligned}\mathbb{E}\left[b^{\bar{\ell}+\Delta\ell}_{\bar{\ell}+\Delta\ell}(b^{\bar{\ell}+2\Delta\ell}_{\bar{\ell}})^*\right]\simeq&\exp\left(-\frac{D\tau}{4\hbar^2}\left[1-\text{sinc}\left(2\Delta\ell\omega_r\tau\right)\right]\right)\\&\times\exp\left[i\frac{\omega_r\tau}{2}\Delta\ell(2\bar{\ell}+\Delta\ell)\right].\end{aligned} \tag{S52}$$

Putting everything together, we obtain the measurement signal

$$P(D)=\frac{1}{2}-\frac{1}{2}\cos\left(\omega_r\tau\Delta\ell^2\right)C(\tau), \tag{S53}$$

with the reduction factor of the Ramsey fringe contrast due to rotational decoherence

$$C(\tau)=\exp\left(-\frac{D\tau}{2\hbar^2}\left[1-\text{sinc}\left(2\Delta\ell\omega_r\tau\right)\right]\right). \tag{S54}$$

## II. COHERENT EFFECTS ON THE CONTRAST DECAY PROFILE

From (S53) we see that the phase contrast, which decays from decoherence as $C(\tau)$ given by (4) in the main text, is additionally modulated by a factor

$$C_{\text{mod}}(\tau)=\cos\big(\omega_r\Delta\ell^2\tau\big). \tag{S55}$$

This arises from interference between the two relevant coherences of the rotor state: $|\ell\rangle\leftrightarrow|\ell+\Delta\ell\rangle$ and $|\ell+\Delta\ell\rangle\leftrightarrow|\ell+2\Delta\ell\rangle$, whose respective transition frequencies differ by $2\Delta\ell^2\omega_r=2\pi\times 26\,\text{Hz}\times\Delta\ell^2$. This modulation is necessarily present in the coherence measurements presented in this work, which otherwise yield a contrast profile of the form $\exp\big[-(\gamma\tau)^3\big]$. Equation (S55) predicts a node in the fringe contrast at $\tau=\pi/(2\Delta\ell^2\omega_r)$. The modulation may therefore be safely neglected only if the coherence time is much shorter than the node time, $1/\gamma\ll\pi/(2\Delta\ell^2\omega_r)$. Otherwise, the effect of the modulation may be measurable before decoherence has occurred, and thus this effect must be accounted for in order to accurately estimate $\gamma$ from the measurements. We find from numerical simulations that the modulation profile may be appreciably influenced by imperfect operations, where only a partial initial coherence is created, which we therefore must also take into account.

Figure 2 demonstrates this effect. Measured contrast decay curves for $\Delta\ell=3$ superpositions are shown, whose fits for $\gamma$ are shown in Fig. 3(b). The shaded region shows the profile $C_{\text{mod}}(\tau)$, modified from (S55) to account for imperfect operations (sub-unity initial contrast)

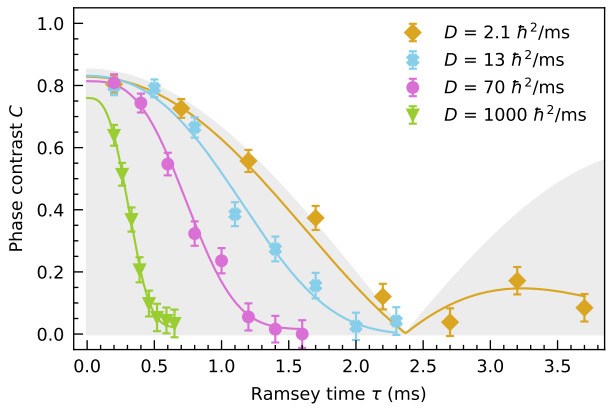


FIG. 2. Coherent oscillations of phase contrast amplitude. All contrast decay measurements for $\Delta\ell = 3$ measurements of decoherence presented in Fig. 3(b) are shown here. The shaded region is the contrast profile of the coherent effect discussed in this section. Solid lines are fits of the form (5) from the main text, additionally multiplied by the shaded profile only if $\Delta\ell^2\omega_r/2\pi\gamma > 0.1$. In these cases, the coherence time is sufficiently long that the effect is appreciable. Here, this applies to only the $D = 2.1\,\hbar^2/\mathrm{ms}$ and $D = 13\,\hbar^2/\mathrm{ms}$ curves.

such that it yields agreement with numerical simulations. In particular, (S55) predicts a node in the contrast at $\tau = \pi/(2\Delta\ell^2\omega_r) = 2.1\,\mathrm{ms}$, while the numerically simulated profile corrected for imperfect operations predicts this node to instead be at $t = 2.4\,\mathrm{ms}$, as shown in Fig 2. If the coherence time is comparable or greater than this node time, then the measured decay profile differs significantly from (5) from the main text, and must be accounted for when extracting a decoherence rate. Including corrections due to imperfect operations, the contrast node is expected to occur at $\tau = 4.8\,\mathrm{ms}$ for our $\Delta\ell = 2$ measurements, and at $\tau = 19\,\mathrm{ms}$ for our $\Delta\ell = 1$ measurements. For most of our measurements, this effect is negligible. In estimating the decoherence rate $\gamma$ in Fig. 3(b), we explicitly account for this effect only when $\Delta\ell^2\omega_r/2\pi\gamma > 0.1$.

## III. NON-RIGID EFFECTS

In the main text, we approximate the ion crystal as a rigid rotor. The leading-order non-rigid effect is centrifugal distortion: the moment of inertia increases as the square of the rotation frequency due to centrifugal force, effectively reducing the rotational constant $\omega_r$ with increasing angular momentum. For an in-plane confinement strength such that the center-of-mass vibrational frequency is $\omega_x$, the fractional change to $\omega_r$ due to finite rotation frequency $\omega_{\mathrm{rot}}$ is given by $2\omega_{\mathrm{rot}}^2/\omega_x^2 = 2.0\times10^{-2}$ for parameters used in this work. This quantity is smaller than the fractional uncertainty of any measurement presented, so we neglect this correction.

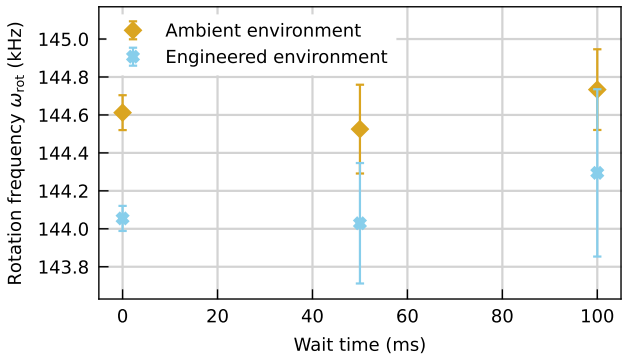


FIG. 3. Measurements of rotational friction. The rotation frequency is measured as a function of wait time after preparation of a rapidly rotating state, both without without ($D = 19\,\hbar^2/\mathrm{ms}$) and with ($D = 110\,\hbar^2/\mathrm{ms}$) voltage noise injection. Over 100 ms, no measurable slowdown is observed.

## IV. MEASUREMENTS OF ROTATIONAL FRICTION

A finite-temperature environment interacting with a quantum rotor will have a frictional effect in addition to angular momentum diffusion, which in general may affect the decoherence dynamics [45]. We thus verify that the environment is well-approximated as infinite temperature by confirming that rotational friction is negligible. We measure rotational friction by recording the center frequency of a rotational sideband at various wait times after rotational state preparation. For increased sensitivity, the third rotational sideband frequency $\omega_{sb}^{(\Delta\ell=3)}$ is chosen, and the rotation frequency inferred as $\omega_{\mathrm{rot}} = \omega_{sb}^{(\Delta\ell=3)}/3$. As shown in Fig. 3, we do this for both an ambient environment ($D = 19\,\hbar^2/\mathrm{ms}$) and an engineered environment ($D = 110\,\hbar^2/\mathrm{ms}$). In both cases, we find the rate of slowdown to be consistent with zero. We bound the rate of slowdown ($2\sigma$ uncertainty of the slope of the fit) at $< 0.2\,\hbar/\mathrm{ms}$ in the case of the ambient environment, and $< 0.3\,\hbar/\mathrm{ms}$ in the case of the engineered environment. We thus neglect rotational friction in the theoretical treatment in the main text.

## V. ADDITIONAL DECOHERENCE SOURCES

Two other potentially relevant effects are decoherence of the ions' electronic state and changes of the rotor's moment of inertia due to fluctuations of the trap frequency. We rule out both of these as significant contributions.

Since the Ramsey experiment entangles the angular

momentum state of the rotor with the electronic state of the ions, decoherence of the electronic states will also result in a loss of measured phase contrast. To measure the electronic coherence time, we trap a single ion and prepare it in the superposition $|S\rangle + |D\rangle$ with a Ramsey experiment including a Hahn echo pulse. This measurement is shown in Fig. 4, where we find the $1/e$ coherence time to be 38 ms, much longer than any coherence measurement presented in this work.

Changes in the rotor's moment of inertia conserve its angular momentum but change the rotation frequency, thereby also decohering a superposition of angular displacements. The stability of the moment of inertia $I$ is determined by the stability of the transverse trap frequency $\omega_x$, related by $I \propto \omega_x^{-4/3}$. We measure the stability of the trap frequency by trapping a single ion and preparing it in the Fock-state superposition $|0\rangle + |1\rangle$ with a Ramsey experiment including a Hahn echo pulse. We find that this vibrational motion has a $1/e$ coherence time of 32 ms, as shown in Fig. 4. When propagated to the case of angular momentum superpositions in the rotor for $\omega_{\mathrm{rot}} = 145$ kHz, this yields an inferred rotational coherence time of $240\,\mathrm{ms}/\Delta\ell$, again much longer than the actual rotational coherence times measured.

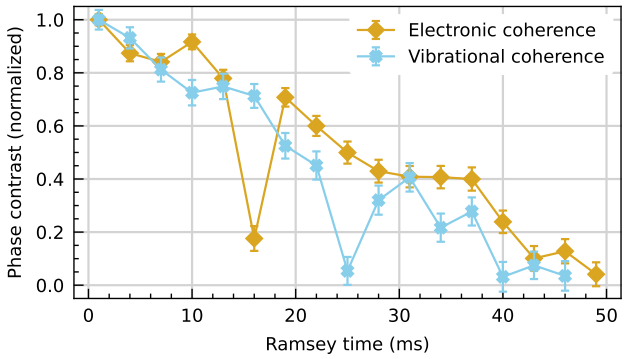


FIG. 4. Measurements of other coherences. The electronic coherence measurement measures the coherence of the superposition $|S\rangle + |D\rangle$ of a single ion, and the motional coherence measurement measures the coherence of horizontal vibrational motion of a single ion, placing a bound on the stability of the rotor's moment of inertia. A Hahn echo pulse is included in both of these measurements to match the conditions of the rotational decoherence measurements.